Mon. Not. R. Astron. Soc. **000**, 1–5 (2010) Printed 23 June 2010 (MN LATEX style file v2.2)

2M1938+4603: A rich, multimode pulsating sdB star with an eclipsing dM companion observed with *Kepler*

R. H. Østensen,[1⋆] E. M. Green,[2] S. Bloemen,[1] T. R. Marsh,[3] J. B. Laird,[2] M. Morris,[2] E. Moriyama,[2] R. Oreiro,[4] M. D. Reed,[5] S. D. Kawaler,[6] C. Aerts,[1,7] M. Vučković,[8] P. Degroote,[1] J. H. Telting,[9] H. Kjeldsen,[10] R. L. Gilliland,[11] J. Christensen-Dalsgaard,[10] W. J. Borucki[12] and D. Koch[12]

[1] *Instituut voor Sterrenkunde, K. U. Leuven, Celestijnenlaan 200D, 3001 Leuven, Belgium*
[2] *Steward Observatory, University of Arizona, 933 N. Cherry Ave., Tucson, AZ 85721, USA*
[3] *Department of Physics, University of Warwick, Coventry CV4 7AL, UK*
[4] *Instituto de Astrofísica de Andalucía, Glorieta de la Astronomía s/n, 18008 Granada, Spain*
[5] *Department of Physics, Astronomy, and Materials Science, Missouri State University, Springfield, MO 65804, USA*
[6] *Department of Physics and Astronomy, Iowa State University, Ames, IA 50011, USA*
[7] *Department of Astrophysics, IMAPP, Radboud University Nijmegen, 6500 GL Nijmegen, The Netherlands*
[8] *European Southern Observatory, Alonso de Córdova 3107, Vitacura, Casilla 19001, Santiago, Chile*
[9] *Nordic Optical Telescope, 38700 Santa Cruz de La Palma, Spain*
[10] *Department of Physics and Astronomy, Aarhus University, 8000 Aarhus C, Denmark*
[11] *Space Telescope Science Institute, 3700 San Martin Drive, Baltimore, MD 21218, USA*
[12] *NASA Ames Research Center, MS 244-30, Moffett Field, CA 94035, USA*

Released 2010 Xxxxx XX

ABSTRACT

2M1938+4603 (KIC 9472174) displays a spectacular light curve dominated by a strong reflection effect and rather shallow, grazing eclipses. The orbital period is 0.126 days, the second longest period yet found for an eclipsing sdB+dM, but still close to the minimum 0.1-d period among such systems. The phase-folded light curve was used to detrend the orbital effects from the dataset, and the resulting amplitude spectrum shows a rich collection of pulsation peaks spanning frequencies from ∼50 to 4500 μHz. The presence of a complex pulsation spectrum in both the *p*-mode and the *g*-mode regions has never been seen before in a compact pulsator.

Eclipsing sdB+dM stars are very rare, with only seven systems known and only one with a pulsating primary. Pulsating stars in eclipsing binaries are especially important since they permit masses derived from seismological model fits to be cross checked with orbital mass constraints. We present a first analysis of this star based on the *Kepler* 9.7-day commissioning light curve and extensive ground-based photometry and spectroscopy that allow us to set useful bounds on the system parameters. We derive a radial-velocity amplitude $K_1 = 65.7 \pm 0.6\,\mathrm{km\,s^{-1}}$, inclination angle $i = 69.45 \pm 0.20\,^{\circ}$, and find that the masses of the components are $M_1 = 0.48 \pm 0.03\,\mathrm{M}_{\odot}$ and $M_2 = 0.12 \pm 0.01\,\mathrm{M}_{\odot}$.

Key words: subdwarfs – binaries: close – binaries: eclipsing – stars: variables: general – stars: individual: 2M1938+4603

1 INTRODUCTION

The subdwarf B (sdB) stars are known to be core helium burning stars with extremely thin ($\mathrm{M_{env}} \leqslant 0.01\,\mathrm{M}_{\odot}$) inert hydrogen dominated envelopes (Heber 1986). This places them on an extension to the classical horizontal branch, known as the extreme horizontal branch (EHB). In order to reach this configuration, almost the entire envelope must be stripped off close to the tip of the red giant branch. There are several binary scenarios that are capable of accomplishing this, such as common-envelope ejection (CEE), stable Roche-lobe overflow and merger of two helium-core white dwarfs (Han et al. 2002). A small minority of sdB stars in the field are found to have close M-dwarf companions (see

⋆ E-mail: roy@ster.kuleuven.be

For et al. 2010, for recent results and a review), and seven such systems are eclipsing. The eclipsing systems have been monitored over long time-bases in order to detect low-mass companions from precise measurements of the eclipse timings with the O–C method (Kilkenny et al. 2003; Lee et al. 2009).

One of the eclipsing sdB+dM systems, NY Vir, has a pulsating primary of the V361 Hya class (Kilkenny et al. 1998). The V361 Hya stars were discovered by Kilkenny et al. (1997) and are characterised by rapid pulsations, typically in the period range between two and five minutes. They are known to be pressure (p-)mode pulsators excited by the κ mechanism, driven primarily by an iron opacity bump in the envelope (Charpinet et al. 1997). A second class of sdB pulsators was reported by Green et al. (2003). These stars, now known as V1093 Her stars, show pulsations with much longer periods ($\sim$1 h) than the V361 Hya stars, and their temperatures are lower. These pulsations can be described in terms of gravity (g-)modes excited by the same κ mechanism (Fontaine et al. 2003). With the discovery of long-period pulsations in a known rapid pulsator, DW Lyn, Schuh et al. (2006) established the existence of hybrid sdB pulsators. A broad review of hot subdwarf stars in general can be found in Heber (2009), and a review of asteroseismology and evolution of the EHB stars can be found in Østensen (2009). For the most recent pulsator discoveries see Østensen et al. (2010a).

The *Kepler* spacecraft was launched in March 2009, aiming to find Earth-sized planets from photometric observations of a 105 square degree field (Borucki et al. 2010). *Kepler* is also ideally suited for asteroseismological studies, and the Kepler Asteroseismic Science Consortium (KASC, Gilliland et al. 2010) manages this important aspect of the mission. The methods with which the compact pulsator candidates were selected, together with analysis of the first half of the survey phase, are presented in Østensen et al. (2010b, Paper I). The first results on a V361 Hya star in the *Kepler* field are presented by Kawaler et al. (2010a), the first results on V1093 Her and DW Lyn pulsators are presented by Reed et al. (2010), and results on two V1093 Her pulsators in sdB+dM reflection binaries are discussed in Kawaler et al. (2010b). Further analysis of *Kepler* data on sdB stars are found in Van Grootel et al. (2010), who present the first detailed asteroseismic analysis of a V1093 Her star, and in Bloemen et al. (2010), who present a detailed analysis of the extraordinary binary light curve of the sdB+WD star KPD 1946+4340.

In this letter we present 2M1938+4603 (KIC 9472174), an object first identified as an sdB star in the *Kepler* field during a survey of blue targets selected from 2MASS photometry (Skrutskie et al. 2006). Follow-up photometry showed the presence of a reflection effect with shallow primary and secondary eclipses (Fig. 1). The amplitude of the reflection effect is very comparable to those observed in HW Vir and NY Vir, but the eclipses are much more shallow. After detrending the *Kepler* light curve, we clearly detect low-level pulsations.

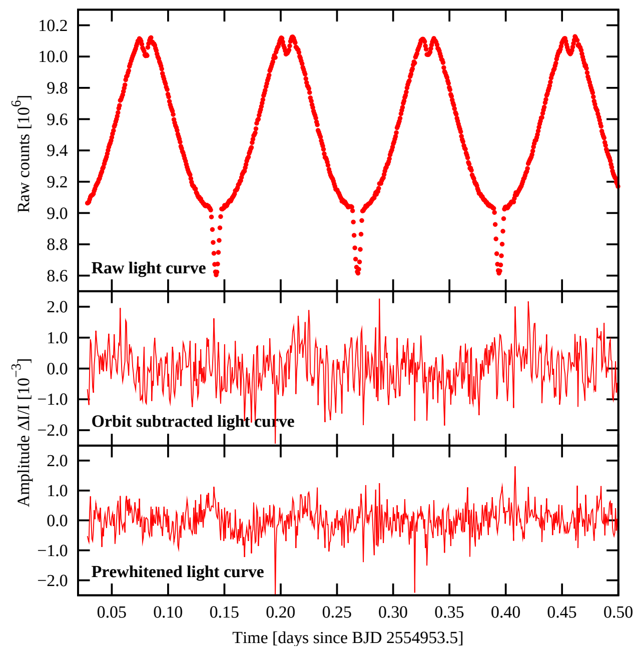

Figure 1. The first half day of the *Kepler* light curve. The upper panel shows the raw data, which is dominated by the strong reflection effect, with both primary and secondary eclipses clearly visible. The middle panel shows the same chunk after detrending with the light curve folded on P, and the bottom panel shows the same after prewhitening the 55 most significant frequencies.

2 OBSERVATIONS

The discovery of the strong reflection effect with grazing eclipses was made by two of us (JBL & MM) during a photometric run in June 2008. Here we present only the eclipse timings from the ground-based photometry, as the pulsations are too complex and have too low amplitudes to be significant in those light curves. The times of thirteen primary eclipses collected between June 2008 and May 2010 (Table A1) give the following ephemeris:

$$T_0 = 2454640.864162 \pm 0.000058\,\mathrm{d}$$
$$P = 0.125765300 \pm 0.000000021\,\mathrm{d}.$$

We downloaded the *Kepler* Q0 light curve from the KASC archive, corrected the raw time-stamps to Barycentric Julian Date (BJD) according to the instructions (Van Cleve 2009), and made minor corrections to the raw fluxes to take out trends on time-scales longer than a day. The 77 consecutive eclipse times measured from the *Kepler* photometry are listed in Table A2, and match the ground-based ephemeris well within the errors.

In order to produce a useful Fourier Transform (FT) that shows the spectrum of low-level pulsations in 2M1938+4603 among the extremely dominant orbital effects (Fig. 1, top panel) we first attempted to clean out a model light curve of the system, but we abandoned this approach since the FT of the residuals contain significant peaks at *every* orbital harmonic. The model light curve is unable to produce a satisfactory fit to the complicated irradiation effect, at the exceptional precision of the *Kepler* photometry. Our model light curve does not account for radiative transfer through the heated face of the M-dwarf, which may account

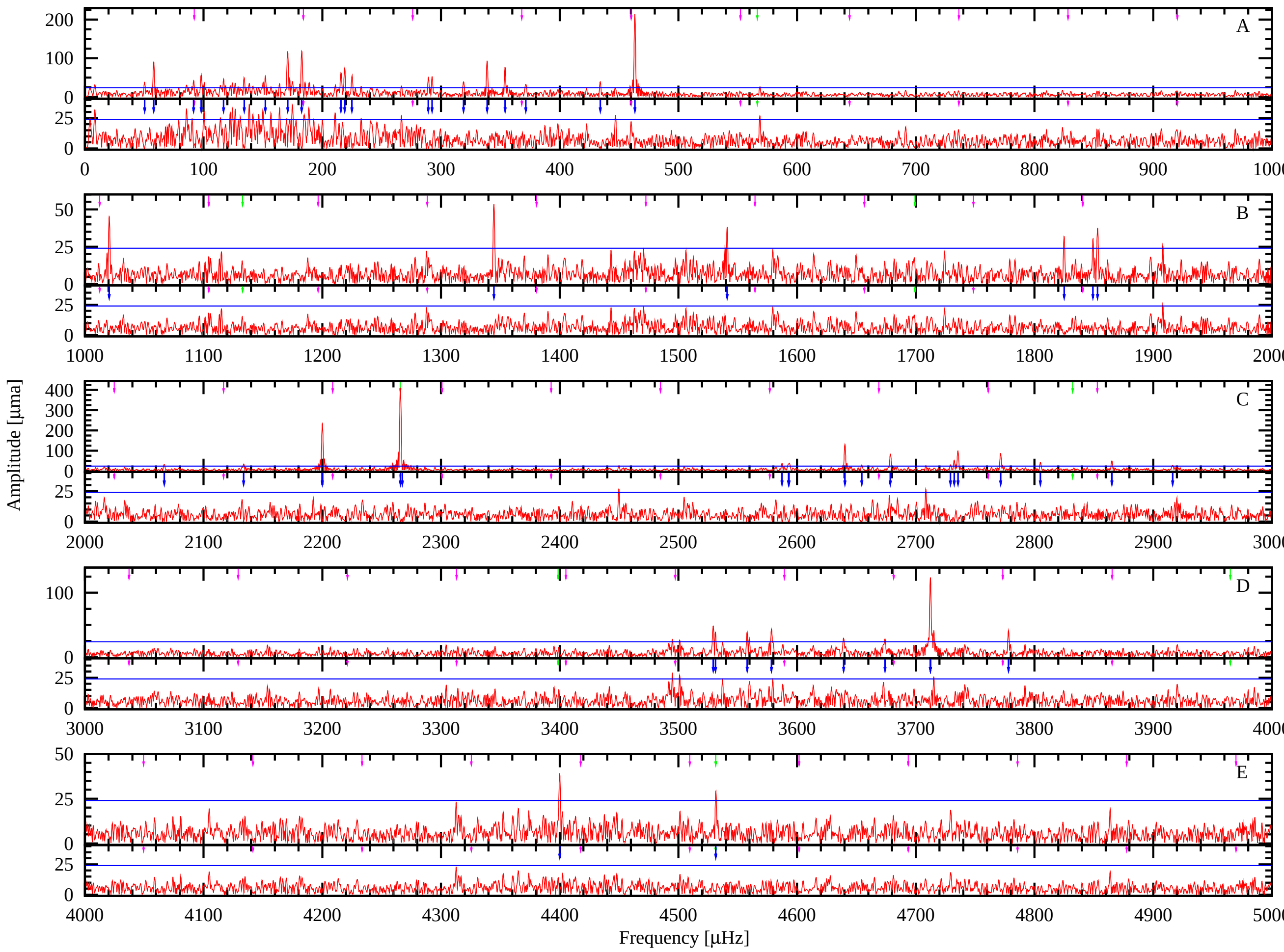

Figure 2. The FT of the data after detrending the orbital and long term variations (upper part of each panel). The panels are labeled A, B, C, D, E and these also define the group designation used in Table D1. The magenta arrows indicate the orbital frequency of $f_{\rm orb} = 92$ μHz and all its harmonics, which have been completely removed by subtracting the data folded $f_{\rm orb}$. The green arrows indicate the *Kepler* long-cadence cycle, $f_{\rm lc}$ and its harmonics, at which possible artefacts are known to be found. The lower part of each panel shows the FT of the data after prewhitening 55 frequencies, as marked with blue arrows. The blue line indicates four times the mean noise level at 24 μma.

for some of the discrepancies between the model and data. Until such issues are resolved the precise parameters of our model are subject to systematic uncertainties that could well be in excess of the statistical errors. Even if we managed to model all orbital effects in the light curve to the required precision, any pulsation peaks found in the residuals on an orbital harmonic frequency would still be suspicious. So instead we proceeded by folding the *Kepler* light curve on P, and then using the result to clean out all orbital effects from the light curve. Note that any stable pulsations that coincide with these periods within the resolution are also very effectively removed.

2.1 Frequency determination

After removing the orbital effects from the light curve, a spectacularly rich pulsation spectrum is revealed (upper half of the five panels in Fig. 2). We have identified 55 frequencies between ∼50 and 4500 μHz that have amplitudes well above four times the mean level of 6 μma[1] computed from the whole FT between 500 μHz and the Nyquist frequency, $f_{\rm Nyq} = 8496$ μHz. These frequencies are listed in Table D1. Several more frequencies remain above the 24 μma limit, after prewhitening the light curve with these 55 frequencies (lower half of the panels in Fig. 2), especially in the low frequency region below 500 μHz. However, we chose to constrain ourselves to the most clearly resolved peaks in this first analysis, as much more *Kepler* data is underway, and will provide a tenfold increase in resolution and a threefold drop in the noise level after only the first three-month cycle of observations. In total we hope to obtain close to five years of almost continuous space based observations on this object, so we will limit ourselves to discussing only the most obvious features here.

The FT shows several distinct groups of frequencies, and we number the frequencies in each group separately

[1] One micro-modulation amplitude (μma) is equivalent to a semi-amplitude of one part per million of the mean light level.

as A, B, C, D, E, as indicated in Fig. 2. The frequencies in group A are typical for the V1093 Her stars, and we identify and remove 20 peaks, with the lowest at $6\,\sigma$. There are clearly many more frequencies than this, in particular between 100 and 200 μHz, but the resolution is not good enough to justify pushing the limit further. There are no significant frequencies between 500 and 1000 μHz, except one at 570 μHz which is just above the detection limit. Note also that this frequency is close to the long cadence readout cycle at $f_{\rm lc} = 566.4$ μHz. In group B we find only six rather low-level peaks. Group C contains the strongest peak in the FT at $f_{C4} = 2265.8$ μHz with an amplitude of 423 μma. This frequency is almost exactly at $4f_{\rm lc} = 2265.4$ μHz, but since we do not observe such strong artefacts in any other stars we are inclined to believe that this is a real pulsation mode. In all other short cadence *Kepler* datasets we have worked with, the strongest artefact peak is found at 8 or $9f_{\rm lc}$. In this dataset $9f_{\rm lc}$ is not present at all, and $8f_{\rm lc} = 4531$ μHz is barely above the detection limit, while f_{C4} is 70-σ! The second strongest peak in the FT is also found right next to it, $f_{C3} = 2200.1$ μHz with an amplitude of 233 μma. Another rich set of peaks is found around 2700 μHz, so that group C contains 18 peaks altogether. Group D contains 9 clear peaks between 3500 and 3800 μHz, and group E contains only two significant peaks located at $2f_{C3}$ and $2f_{C4} = 8f_{\rm lc}$. The ratio of some of the high-amplitude peaks in the short-period range, such as $f_{D7}/f_{C4} = 1.638$ and $f_{D9}/f_{C3} = 1.717$, which are both close to the theoretical ratio of the radial fundamental and the second overtone (1.667), and a stellar model for the $T_{\rm eff}$ and $\log g$ of the primary does display pulsation periods for radial modes close to these frequencies.

The frequency analysis and error estimations on the parameters are done as outlined in Degroote et al. (2009). Because some of the frequencies were closer together than the Rayleigh T^{-1} limit, and thus unresolved, we have performed additional analyses, where after each prewhitening stage, some of the frequencies, amplitudes and phases were refitted with a Levenberg–Marquardt nonlinear fitting routine. To investigate the stability of the fit and the differences from the linear analysis, we first only updated the amplitudes, phases and frequencies belonging the last two identified peaks, then updating the parameters belonging to the last 20 peaks, and finally using all identified frequencies. The differences between the amplitudes and frequencies were all within the derived error estimates, except for the frequencies around 3712 and 2593 μHz. The nonlinear fitting algorithm did not produce consistent results at these frequencies, but future observations will allow us to resolve these structures. Below 200 μHz, a dense forest of barely significant peaks is visible. Although the different methods give consistent results, more *Kepler* photometry will be necessary to fully resolve them.

2.2 Spectroscopy

Spectroscopic observations to determine radial velocities for 2M1938+4603 were undertaken primarily with the B&C spectrograph on the 2.3-m *Bok Telescope* on Kitt Peak. A few spectra were also obtained using the MMT Blue spectrograph. In both cases, an 832/mm grating was employed in second order, and particular care was taken to maintain precise centering of the star on the slit throughout the exposures. The resulting spectra have a resolution of $R \sim 2150$ over the range 3675 – 4520 Å (Bok), or $R \sim 4200$, 4000 – 4950 Å (MMT). Radial velocities were derived by cross-correlating the individual continuum-removed spectra against a super-template using the IRAF task `FXCOR`. The super-template for the lower resolution spectra was obtained by shifting the 66 individual spectra to the same velocity prior to median filtering into a single spectrum; the velocity zero point of the resulting template was thus undetermined. The cross-correlation template for the 6 MMT spectra was constructed from 19 spectra previously obtained with the identical spectroscopic setup for other hot subdwarfs of known radial velocities, whose spectral abundance patterns closely match that of 2M1938+4603.

A single sinusoidal fit was performed to all 72 velocities as a function of orbital phase, weighted by the velocity errors and also including an additional term for the zero-point offset of the Bok velocities relative to the MMT velocities (Fig. B1). The orbital period was fixed at the value of 0.12576530 d derived from the eclipse timings. The derived RV semi-amplitude is $K_1 = 65.7 \pm 0.6\,{\rm km\,s^{-1}}$, with a systemic velocity $\gamma = 20.1 \pm 0.3\,{\rm km\,s^{-1}}$.

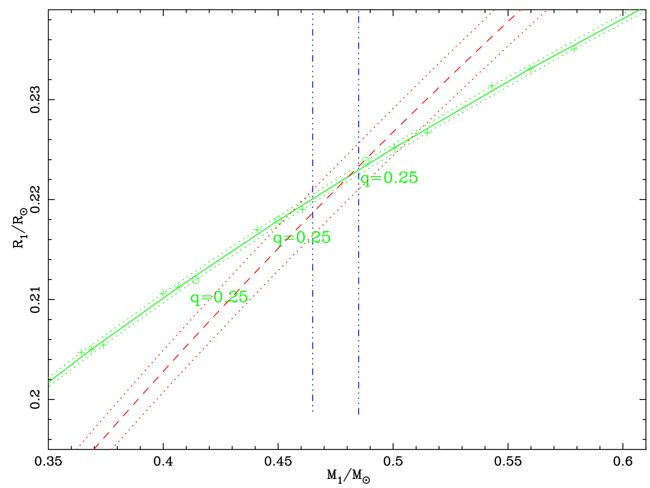

Figure 3. Mass–radius diagram for 2M1938+4603 showing the regions permitted by the orbit solution (green curves) and by the spectroscopic gravity (red curves). The dotted, green curves show the error ranges that corresponds to a 3-σ error in K_1 for the orbit solution. The dotted, red curves corresponds to the one σ formal error on $\log g$ for the gravity track. The green curves are labeled with the value for $q = M_1/M_2$ that corresponds to each point on the curve, with + marking ticks of 0.01, increasing to the left. Note that changing K_1 by 3σ shifts the curve very little in the M/R plane, but the q-value changes considerably. Vertical lines show the mass range typical for canonical EHB stars formed through the CE channel.

3 SYSTEM PARAMETERS

The effective temperature, surface gravity, and helium abundance of 2M1938+4603 were determined in the context of Paper I to be $T_{\rm eff} = 29\,564 \pm 106$ K, $\log g = 5.425 \pm 0.009$ dex, and $\log(N_{\rm He}/N_{\rm H}) = -2.36 \pm 0.06$ dex, using metal blanketed LTE models. This temperature is close to the boundary region between the p- and g-mode pulsators, where hybrid DW Lyn type pulsators have been found.

We modelled the light curve using grid elements covering each star, accounting for tidal (ellipsoidal) distortion of each star and gravity and limb-darkening of the sdB as in Bloemen et al. (2010). Irradiation of the M-dwarf was accounted for by summing the M-dwarf flux with the incident flux from the sdB point by point. Surface brightnesses were computed assuming black-body spectra at a single wavelength of 600 nm. The best fitting model is found to have the following parameters: inclination angle, $i = 69.45(2)^{\circ}$, relative radii, $r_1 = 0.250(1)$, $r_2 = 0.177(1)$ in units of the orbital separation. The errors in parentheses are formal fitting errors that may underestimate the true errors perhaps as much as a factor 10, considering the discrepancies in the light curve fitting. The high precision on these parameters allows us to use the mass-radius relationships as derived from the orbital parameters and from the surface gravity to constrain the mass and radius of the primary, as shown in Fig. 3. We clearly see that the permitted M/R given by the photometric orbital parameters (P, i, r_1 and r_2) and the spectroscopic K_1 crosses the M/R given by the spectroscopic surface gravity at precisely the expected primary mass for a post-CE sdB star. The adjacent dotted lines indicate the errors (on the RV for the q-track, and on $\log g$ for the g-track since the errors on P, i and the relative radii are too small to matter). A mass for the primary of $M_1 = 0.48 \pm 0.03\,\mathrm{M}_{\odot}$ can be deduced from the diagram. Using K_1 and P we know the mass function $f(M) = 0.003695$. With $0.48\,\mathrm{M}_{\odot}$ for the primary, and solving for the secondary, we get $M_2 = 0.12 \pm 0.01\,\mathrm{M}_{\odot}$.

4 DISCUSSION AND OUTLOOK

We have presented the discovery of a new eclipsing sdB with an M-dwarf companion, and demonstrated that the primary is an unusual pulsator with frequencies spanning the range from 50 to 4400 μHz. The unprecedented precision of the *Kepler* observations makes a direct comparison to other known eclipsing sdB+dM systems rather difficult, since such low-level pulsations as we find in 2M1938+4603 would be undetectable from the ground. Nevertheless, it is an amazing stroke of luck to find an eclipsing sdB+dM system within the narrow confines of the *Kepler* field, especially one as bright as 12th magnitude, considering the fact that only seven such systems are known among the thousands of subdwarfs that have been surveyed for variability to date.

In future papers we will produce a more realistic model that can handle the irradiation effect of the M-dwarf to improve the binary light curve model, and produce asteroseismic models that can reproduce the frequencies observed in this star. When longer time-series of *Kepler* photometry become available, we will be able to fully resolve the densely packed amplitude spectrum that we see in the g-mode region between 100 and 200 μHz. This will enable us to produce an asteroseismic model reproducing all the frequencies in this complex rotating pulsator, as was done for NY Vir by Charpinet et al. (2008). Since 2M1938+4603 has g-modes in addition to p-modes we should also be able to constrain the deeper structure of the sdB core, and hopefully also establish the mass of its progenitor, before the envelope was ejected by the companion. With five years of precise eclipse timings we may detect planetary companions from variations in the O–C diagram, if they orbit this compact binary with periods shorter than the *Kepler Mission*, and the low-amplitude pulsations are found to be stable on such time-scales.

ACKNOWLEDGMENTS

The authors gratefully acknowledge the *Kepler* team and everybody who has contributed to making this mission possible. Funding for the *Kepler Mission* is provided by NASA's Science Mission Directorate.

Part of the spectroscopic observations reported here were obtained at the MMT Observatory, a joint facility of the University of Arizona and the Smithsonian Institution.

The research leading to these results has received funding from the European Research Council under the European Community's Seventh Framework Programme (FP7/2007–2013)/ERC grant agreement № 227224 (PROSPERITY), as well as from the Research Council of K.U.Leuven grant agreement GOA/2008/04.

REFERENCES

Bloemen S. et al., 2010, MNRAS, submitted, ...
Borucki W. J. et al., 2010, Science, 327, 977
Charpinet S., Fontaine G., Brassard P., Chayer P., Rogers F. J., Iglesias C. A., Dorman B. 1997, ApJ, 483, L123
Charpinet S., van Grootel V., Reese D., Fontaine G., Green E. M., Brassard P., Chayer P. 2008, A&A, 489, 377
Degroote P. et al., 2009, A&A, 506, 471
Fontaine G., Brassard P., Charpinet S., Green E. M., Chayer P., Billères M., Randall S. K. 2003, ApJ, 597, 518
For B.-Q. et al., 2010, ApJ, 708, 253
Gilliland R. L. et al., 2010, PASP, 122, 131
Green E. M. et al., 2003, ApJ, 583, L31
Han Z., Podsiadlowski P., Maxted P. F. L., Marsh T. R., Ivanova N. 2002, MNRAS, 336, 449
Heber U. 1986, A&A, 155, 33
Heber U. 2009, ARA&A, 47, 211
Kawaler S. D. et al., 2010a, MNRAS, submitted, ...
Kawaler S. D. et al., 2010b, MNRAS, submitted, ...
Kilkenny D., Koen C., O'Donoghue D., Stobie R. S. 1997, MNRAS, 285, 640
Kilkenny D., O'Donoghue D., Koen C., Lynas-Gray A. E., van Wyk F. 1998, MNRAS, 296, 329
Kilkenny D., van Wyk F., Marang F. 2003, The Observatory, 123, 31
Lee J. W., Kim S.-L., Kim C.-H., Koch R. H., Lee C.-U., Kim H.-I., Park J.-H. 2009, AJ, 137, 3181
Østensen R. 2009, Communications in Asteroseismology, 159, 75
Østensen R. H. et al., 2010a, A&A, 513, A6
Østensen R. H. et al., 2010b, MNRAS, submitted, ...
Reed M. et al., 2010, MNRAS, submitted, ...
Schuh S., Huber J., Dreizler S., Heber U., O'Toole S. J., Green E. M., Fontaine G. 2006, A&A, 445, L31
Skrutskie M. F. et al., 2006, AJ, 131, 1163
Van Cleve J. E. 2009, Kepler Data Release Notes 2, http://archive.stsci.edu/kepler/release_notes/release_notes2/Data_Release_02_Notes_2009102213.pdf
Van Grootel V. et al., 2010, ApJL, submitted, ...

Table A1. Times of primary minima from ground based observations, and O–C values for $T_0 = 54640.864162$, $P = 0.125765300$.

Epoch	BJD	$\sigma_{\rm BJD}$	O–C
0	54640.86420	0.00004	0.00004
595	54715.69440	0.00004	-0.00012
714	54730.66060	0.00004	0.00001
929	54757.70010	0.00004	-0.00003
2569	54963.95530	0.00004	0.00008
2577	54964.96140	0.00004	0.00006
2712	54981.93960	0.00004	-0.00006
2720	54982.94560	0.00004	-0.00018
2767	54988.85690	0.00004	0.00015
2775	54989.86305	0.00004	0.00018
3434	55072.74210	0.00004	-0.00010
3696	55105.69270	0.00004	-0.00001
5527	55335.96895	0.00004	-0.00003

APPENDIX A: EPHEMERIS

Online material.

Table A2. Times of primary minima from *Kepler* observations, and O–C values for $T_0 = 54640.864162$, $P = 0.125765300$.

Epoch	BJD	$\sigma_{\rm BJD}$	O–C
2487	54953.64250	0.00001	0.00004
2488	54953.76824	0.00001	0.00001
2489	54953.89401	0.00001	0.00002
2490	54954.01972	0.00001	-0.00004
2491	54954.14554	0.00001	0.00001
2492	54954.27131	0.00001	0.00002
2493	54954.39705	0.00001	-0.00001
2494	54954.52283	0.00001	0.00001
2495	54954.64861	0.00001	0.00002
2496	54954.77433	0.00001	-0.00002
2497	54954.90010	0.00001	-0.00002
2498	54955.02588	0.00001	-0.00000
2499	54955.15162	0.00001	-0.00003
2500	54955.27741	0.00001	-0.00000
2501	54955.40317	0.00001	-0.00000
2502	54955.52895	0.00001	0.00000
2503	54955.65467	0.00001	-0.00004
2504	54955.78047	0.00001	-0.00001
2505	54955.90625	0.00001	0.00001
2506	54956.03200	0.00001	-0.00000
2507	54956.15777	0.00001	-0.00000
2508	54956.28355	0.00001	0.00001
2509	54956.40926	0.00001	-0.00004
2510	54956.53506	0.00001	-0.00001
2511	54956.66083	0.00001	-0.00000
2512	54956.78659	0.00001	-0.00001
2513	54956.91237	0.00001	0.00001
2514	54957.03814	0.00001	0.00001
2515	54957.16392	0.00001	0.00003
2516	54957.28972	0.00001	0.00006
2517	54957.41545	0.00001	0.00003
2518	54957.54121	0.00001	0.00002
2519	54957.66696	0.00001	0.00001
2520	54957.79274	0.00001	0.00002
2521	54957.91850	0.00001	0.00001
2522	54958.04428	0.00001	0.00003
2523	54958.17004	0.00001	0.00003
2524	54958.29579	0.00001	0.00001
2525	54958.42152	0.00001	-0.00002
2526	54958.54734	0.00001	0.00003
2527	54958.67311	0.00001	0.00003
2528	54958.79883	0.00001	-0.00001
2529	54958.92465	0.00001	0.00004
2530	54959.05035	0.00001	-0.00002
2531	54959.17612	0.00001	-0.00002
2532	54959.30187	0.00001	-0.00003
2533	54959.42766	0.00001	-0.00001
2534	54959.55344	0.00001	0.00001
2535	54959.67918	0.00001	-0.00001
2536	54959.80498	0.00001	0.00002
2537	54959.93071	0.00001	-0.00001
2538	54960.05651	0.00001	0.00001
2539	54960.18225	0.00001	-0.00001
2540	54960.30802	0.00001	0.00000
2541	54960.43378	0.00001	-0.00001
2542	54960.55957	0.00001	0.00002
2543	54960.68531	0.00001	-0.00001
2544	54960.81113	0.00001	0.00004
2545	54960.93685	0.00001	-0.00000
2546	54961.06262	0.00001	0.00001

Table A3. Times of primary minima from *Kepler* observations, cont.

Epoch	BJD	$\sigma_{\rm BJD}$	O–C
2547	54961.18842	0.00001	0.00004
2548	54961.31416	0.00001	0.00001
2549	54961.43995	0.00001	0.00004
2550	54961.56569	0.00001	0.00001
2551	54961.69145	0.00001	0.00001
2552	54961.81719	0.00001	-0.00002
2553	54961.94298	0.00001	0.00001
2554	54962.06873	0.00001	-0.00001
2555	54962.19452	0.00001	0.00002
2556	54962.32026	0.00001	-0.00001
2557	54962.44603	0.00001	-0.00000
2558	54962.57180	0.00001	0.00000
2559	54962.69755	0.00001	-0.00001
2560	54962.82334	0.00001	0.00001
2561	54962.94909	0.00001	-0.00001
2562	54963.07486	0.00001	-0.00000
2563	54963.20060	0.00001	-0.00002

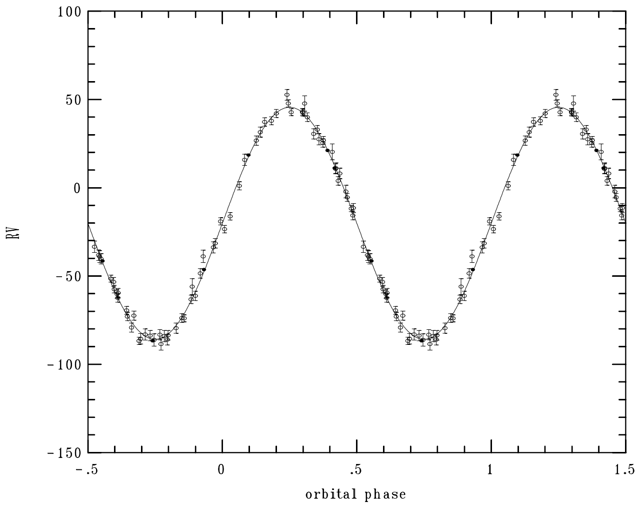

Figure B1. The spectroscopic RVs. Open points are from the *Bok Telescope*, filled dots from the MMT.

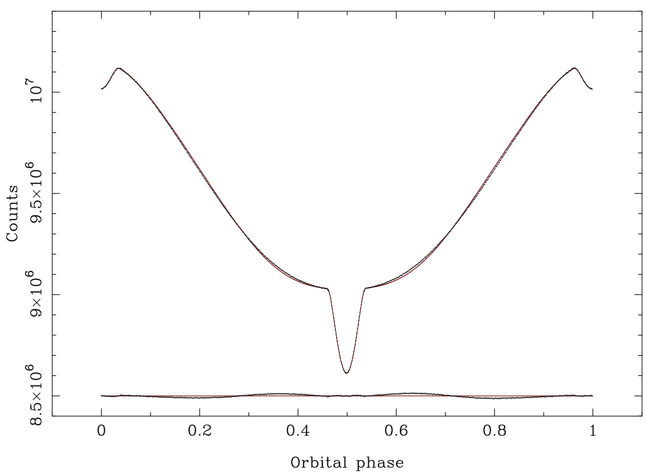

Figure C1. Best fit model light curve and the folded *Kepler* light curve (top), and residuals (bottom).

APPENDIX B: RV MEASUREMENTS

APPENDIX C: LIGHT CURVE MODEL

APPENDIX D: FREQUENCY LIST

The two pairs of frequencies marked with † are unresolved. Prewhitening one frequency with the measured amplitude leaves a significant residual peak, but fitting two frequencies simultaneously produces possibly exaggerated amplitudes and high errors on the frequencies. The amplitude given is therefore only stated as the observed amplitude of the combined peak.

[h!]

Table D1. Clearly resolved frequencies, periods, and amplitudes for 2M1938+4603.

ID	Frequency [μHz]	Period [s]	Amplitude [μma]
f_{A1}	50.289 (137)	19884.934 (54.225)	36 (7)
f_{A2}	57.959 (056)	17253.692 (16.761)	89 (7)
f_{A3}	91.614 (123)	10915.351 (14.709)	40 (7)
f_{A4}	97.954 (089)	10208.828 (09.325)	56 (7)
f_{A5}	116.859 (108)	8557.319 (07.969)	46 (7)
f_{A6}	134.181 (099)	7452.603 (05.500)	50 (7)
f_{A7}	152.043 (090)	6577.086 (03.923)	55 (7)
f_{A8}	170.824 (043)	5853.966 (01.474)	116 (7)
f_{A9}	182.673 (042)	5474.256 (01.260)	119 (7)
f_{A10}	215.762 (085)	4634.736 (01.834)	59 (7)
f_{A11}	218.939 (070)	4567.474 (01.472)	72 (7)
f_{A12}	224.989 (096)	4444.656 (01.898)	52 (7)
f_{A13}	289.349 (113)	3456.036 (01.352)	45 (7)
f_{A14}	292.537 (102)	3418.370 (01.201)	49 (7)
f_{A15}	319.054 (121)	3134.262 (01.191)	41 (7)
f_{A16}	338.857 (054)	2951.098 (00.472)	92 (7)
f_{A17}	353.995 (066)	2824.900 (00.533)	75 (7)
f_{A18}	371.400 (153)	2692.512 (01.113)	32 (7)
f_{A19}	434.133 (129)	2303.443 (00.688)	38 (7)
f_{A20}	463.297 (023)	2158.441 (00.108)	214 (7)
f_{B1}	1020.507 (110)	979.906 (00.106)	45 (7)
f_{B2}	1344.545 (093)	743.746 (00.052)	53 (7)
f_{B3}	1541.048 (131)	648.909 (00.055)	38 (7)
f_{B4}	1824.991 (158)	547.948 (00.048)	31 (7)
f_{B5}	1849.248 (164)	540.760 (00.048)	31 (7)
f_{B6}	1853.196 (134)	539.608 (00.039)	37 (7)
f_{C1}	2066.784 (156)	483.843 (00.037)	32 (7)
f_{C2}	2133.776 (155)	468.653 (00.034)	32 (7)
f_{C3}	2200.061 (021)	454.533 (00.004)	233 (7)
f_{C4}	2265.789 (016)	441.347 (00.003)	423 (7)
f_{C5}	2267.414 (110)	441.031 (00.022)	63 (7)
f_{C6}	2587.292 (150)	386.504 (00.022)	34 (7)
$f_{C7}{}^{\dagger}$	2592.837 (134)	385.678 (00.020)	40 (8)
$f_{C8}{}^{\dagger}$	2593.186 (134)	385.626 (00.020)	– (–)
f_{C9}	2640.303 (037)	378.744 (00.005)	133 (7)
f_{C10}	2654.473 (172)	376.723 (00.024)	29 (7)
f_{C11}	2678.609 (059)	373.328 (00.008)	84 (7)
f_{C12}	2729.208 (142)	366.407 (00.019)	35 (7)
f_{C13}	2732.322 (103)	365.989 (00.014)	49 (7)
f_{C14}	2735.515 (051)	365.562 (00.007)	99 (7)
f_{C15}	2771.443 (056)	360.823 (00.007)	88 (7)
f_{C16}	2805.022 (118)	356.503 (00.015)	42 (7)
f_{C17}	2865.190 (098)	349.017 (00.012)	50 (7)
f_{C18}	2916.403 (176)	342.888 (00.021)	28 (7)
f_{D1}	3529.254 (114)	283.346 (00.009)	45 (7)
f_{D2}	3531.300 (153)	283.182 (00.012)	34 (7)
f_{D3}	3557.908 (130)	281.064 (00.010)	38 (7)
f_{D4}	3578.434 (117)	279.452 (00.009)	43 (7)
f_{D5}	3639.159 (167)	274.789 (00.013)	30 (7)
f_{D6}	3674.105 (166)	272.175 (00.012)	30 (7)
$f_{D7}{}^{\dagger}$	3712.247 (125)	269.379 (00.008)	131 (7)
$f_{D8}{}^{\dagger}$	3712.369 (125)	269.370 (00.008)	– (–)
f_{D9}	3778.092 (119)	264.684 (00.008)	42 (7)
f_{E1}	4400.021 (126)	227.272 (00.007)	39 (7)
f_{E2}	4531.554 (172)	220.675 (00.008)	29 (7)